Decoding sub-seasonal predictors of extreme heat with interpretable machine learning

Jagger Alexander[1], Zong-Liang Yang[1]

[1]Jackson School of Geosciences, Department of Earth and Planetary Sciences, University of Texas at Austin, Austin, TX

Corresponding Author: Jagger Alexander (jaggeralexander@utexas.edu)

In review at Artificial Intelligence for Earth Systems

Abstract

As climate change accelerates, heat waves are becoming more frequent, intense, and deadly. A better understanding of sub-seasonal predictors of extreme heat is crucial for adaptation efforts. This study utilizes an interpretable machine learning model, implementing Extreme Gradient Boosting (XGBoost) with SHapley Additive exPlanations (SHAP), to evaluate the predictive strength of various climate factors—including local weather, global climate indices, geopotential heights, soil moisture, and sea surface temperatures—on heat waves, as classified by consecutive days of extreme daily maximum temperatures across six North American cities over the past 45 years. This model demonstrates strong predictive performance for extreme heat on the sub-seasonal time scale, with sea surface temperatures and soil moisture features emerging as more influential than atmospheric features, though key regional differences in feature importance and feature dependence are shown through variation between chosen cities. Bivariate relationships between MJO phase and amplitude are also uncovered through analysis of model predictions. This method shows promise for rapid application to other regions and also serves as a foundation for integration with dynamical modeling approaches, advancing sub-seasonal extreme heat forecasting more broadly.

Significance Statement

As heat waves intensify with climate change, there is an urgent need for more accurate sub-seasonal forecasts. This research presents a novel machine learning-based method to improve heat wave predictions, offering insights into key drivers of heat on the sub-seasonal scale and enabling earlier, more precise public health interventions that can reduce heat-related illness and mortality.

1. Introduction

Heat waves pose a significant and escalating threat to public health worldwide, with global trends demonstrating increases in their intensity, duration, seasonal length, and frequency due to anthropogenic climate change (Perkins-Kirkpatrick and Gibson 2017). As the rate of heat wave occurrences has accelerated, there has been a clear observed rise in heat-related mortality (Howard et al. 2024). However, forecasting heat waves, especially on sub-seasonal timescales (two weeks to two months) remains a challenge. While there are efforts using dynamical, statistical, machine-learning, and hybrid models for sub-seasonal forecasting efforts, their performance varies, and they are not currently operational for forecasting extreme heat events. Developing reliable methods to forecast these events with extended lead times is critical for enacting timely public health interventions.

This study introduces a machine-learning-based methodology to uncover sub-seasonal predictors of heat waves. Specifically, this approach enables quantification and examination of the drivers of extreme heat on the sub-seasonal timescale, illuminating the specific interactions of various meteorological, land-surface, atmospheric, and ocean processes. This information will not only improve heat wave forecasting but also enhance broader understanding of sub-seasonal weather patterns, identifying areas of focus for future model improvements. By extending the lead time and improving reliability of heat wave forecasts, this research aims to advance early warning systems and support public health strategies to mitigate the adverse effects of extreme heat.

Over the past decade, operational dynamical sub-seasonal forecasts have advanced significantly in skill, application, and utility (White et al. 2022), with the European Centre for Medium-Range Weather Forecasting (ECMWF) extended-range (up to 46 days) ensemble forecasts (Richardson et al. 2020) and the SubX Subseasonal Experiment (Pegion et al. 2019) among the leading efforts. While these models have shown skill in forecasting some extreme weather events (Vitart and Robertson 2018), other events have been dangerously missed beyond three-weeks lead time (Lin et al. 2022). The body of research on sub-seasonal extreme heat forecasting is still limited, restricting its operational use in emergency preparedness. Sub-seasonal climate forecasting is a missing link in developing an early-warning system for heat-related mortality (Lowe et al. 2016), especially given that temperature-related illnesses are largely preventable with timely interventions.

Purely statistical or machine learning-based models for sub-seasonal forecasting of extreme heat have shown considerable skill, often matching or exceeding the performance of dynamical models (Miller et al. 2021; Weirich-Benet et al. 2023). Studies have identified dry soil moisture and persistent atmospheric blocking patterns as key factors for predicting extreme heat events (Wehrli et al. 2019; Lee et al. 2016; Zhang et al. 2023). Recently, hybrid models that integrate dynamical and machine-learning approaches, have demonstrated enhanced predictive skill compared to dynamical models alone (He et al. 2022; Chung et al. 2024; Hwang et al. 2019). However, further refinement in the selection of covariates and methodological approaches is needed to optimize the performance of these hybrid models.

Heat wave characteristics and drivers of heat waves vary by region and individual event (Wehrli et al. 2019; Jiang et al. 2023), underscoring the need for a thorough understanding of region-specific drivers to improve forecast accuracy. While machine learning models have demonstrated skill in sub-seasonal heat wave forecasting (Miloshevich et al. 2023), there are few studies which use these methods to better understand predictors of heat waves across regions. The six cities chosen for this analysis-Austin, TX (Seong et al. 2023; Boumans et al. 2014), Dallas, TX, Houston, TX, Las Vegas, NV, Phoenix, AZ, USA (Habeeb et al. 2015) and Mexico City, Mexico (Vargas and Magaña 2020)- are particularly vulnerable to the health effects of heat waves making them ideal test cases for this novel machine learning-based methodology. The climates of these regions vary dramatically, allowing for a comprehensive assessment of how land surface conditions, oceanic influences, atmospheric dynamics, and broader global climate variability contribute to heat wave formation and intensity. Drying summer soil moisture—a trend expected to persist (Nielsen-Gammon et al. 2020)—plays a crucial role in modulating land-atmosphere feedback, particularly in Austin and Dallas, where reduced evapotranspiration can amplify surface temperatures. The Gulf of Mexico serves as a significant moisture source for Texas cities, modulating heat wave intensity through latent heat flux and atmospheric moisture transport (Kimmel Jr. et al. 2016). Meanwhile, Las Vegas and Phoenix experience extreme dry heat events, driven by persistent high-pressure systems that suppress convection and limit surface cooling (McGregor 2024). Mexico City's heat wave dynamics are shaped by urban heat island effects, altitude-driven atmospheric stability, and regional circulation patterns (Aquino-Martínez et al. 2025). At a broader scale, global climate variability—manifested through modes such as El Niño-Southern Oscillation (ENSO) (Luo and Lau 2020), the Madden-Julian Oscillation (MJO) (Jenney et al. 2019), the Arctic Oscillation (AO), and the North Atlantic Oscillation (NAO) (Yu et al. 2023)—can modulate heat wave frequency and intensity by altering large-scale atmospheric circulation patterns that influence temperature and precipitation anomalies across these regions. By integrating these diverse factors into a machine learning-based methodology, this study aims to improve forecast accuracy and enhance early warning systems tailored to each city's unique climate drivers.

This study aims to assess the predictive skill of these different climate drivers through a machine-learning approach tailored to local heat wave prediction, leveraging a comprehensive range of variables. By examining individual feature impact, we aim to advance sub-seasonal heat wave forecasting in North America, laying the groundwork for future regional hybrid models which integrate machine learning and dynamical approaches.

2. Data and methods

a. Data

This study examines data spanning the heat-wave season (1 June–30 September) over the 45-year period from 1980 to 2024. The extended study duration ensures a robust sample of past heat wave events, although it introduces some variability due to changes in local climate drivers over the study period. Some variables are excluded which exhibit monotonic trends or demonstrate insufficient variability for predictive modeling, such as long-term climate oscillations (e.g., Pacific Decadal Oscillation), change in local vegetation and land-use land-cover. The data included and model generation workflow and shown below (Figure 1).

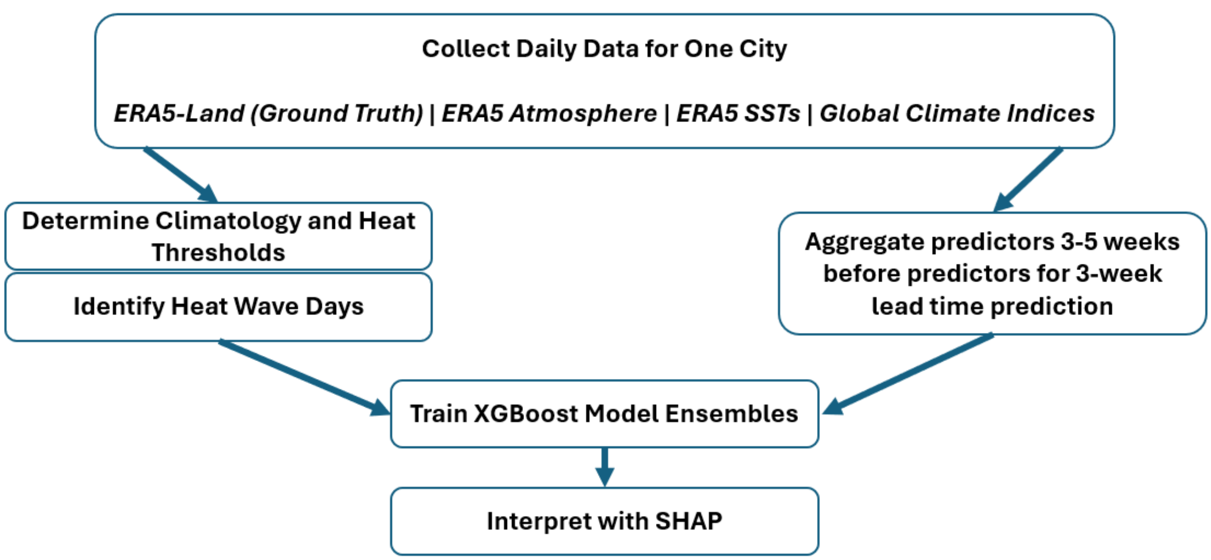

Figure 1. Generalized and simplified workflow for XGBoost sub-seasonal heat wave prediction and interpretation for a single city.

(i) Meteorological and Climatological Data

Meteorological data, including maximum temperature, minimum temperature, relative humidity, surface pressure, 10-meter wind, and total precipitation were obtained from the ERA5-Land reanalysis dataset (Muñoz-Sabater et al. 2021). Observations were extracted for six cities:

- Austin, TX (30.25°N, 97.75°W)
- Houston, TX (29.76°N, 95.37°W)
- Dallas, TX (32.78°N, 96.80°W)
- Phoenix, AZ (33.45°N, 112.07°W)
- Las Vegas, NV (36.17°N, 115.14°W)
- Mexico City, MX (19.43°N, 99.13°W).

Climatological reference values for normal maximum temperature were computed using 30-year means (1980–2010) from ERA5-Land. Mean daily climatological maximum temperature and the standard deviation of day maximum temperature for each day over this thirty-year period were used to calculate a threshold for 90th percentile daily maximum climatology. All climatological data were smoothed with a 14-day running mean to reduce high-frequency variability.

(ii) Oceanic and Climate Variability Data

To assess large-scale climate variability, the study incorporates three global climate indices and information on SSTs in the Niño 3.4 Region:

- MJO Phase and Amplitude: The MJO was quantified on both its phase and amplitude, as derived from the Real-Time Multivariate MJO (RMM) Index (Wheeler and Hendon 2004).
- NAO Index: Daily values of the NAO index were sourced from the NOAA/OAR/PSL dataset (Kalnay et al. 1996).
- AO Index: Daily values of the AO index were sourced from NOAA CPC (NOAA Climate Prediction Center).

- Niño 3.4 Region SSTs: Sea surface temperature (SST) anomalies in the Niño 3.4 region (5°S–5°N, 170°–120°W) were obtained from ERA5 Post-Processed Daily Statistics (Hersbach et al. 2023).

Additionally, two regionally relevant SST variables were included:

- Gulf of Mexico SST: Defined as the mean daily SST within 20°–30°N, 82°–95°W.
- California Current SST: Defined as the mean daily SST within 30°–40°N, 120°–130°W.

Both SST datasets were extracted from ERA5 Post-Processed Daily Statistics.

(iii) Atmospheric Data

Large-scale atmospheric circulation patterns play a crucial role in modulating heat waves at subseasonal timescales (2–6 weeks) (Tuel and Martius 2023). While it is difficult to simply capture large scale atmospheric conditions in a few interpretable features, to account for some key atmospheric drivers of extreme heat, we analyzed four variables from ERA5 hourly single pressure level data (Hersbach et al. 2023):

- 300-hPa U-component of wind
- 300-hPa V-component of wind
- 300-hPa potential vorticity
- 500-hPa geopotential height

Each variable was averaged over a 2.5° latitude–longitude buffer zone surrounding each of the six study cities. The inclusion of these specific fields is motivated by their established relevance in heat wave development. 500-hPa geopotential height serves as a proxy for mid-tropospheric ridging, which is associated with persistent subsidence and warming near the surface (Ventura et al. 2023), 300-hPa U and V wind components characterize upper-level wave patterns and jet stream variability, which influence blocking patterns that contribute to prolonged heat events (Wang et al. 2016). 300-hPa potential vorticity represents upper-tropospheric wave breaking and dynamic forcing mechanisms, which can lead to quasi-stationary ridges that enhance heat wave duration and intensity (Parker et al. 2013). By averaging over a 2.5° spatial buffer, we better capture regional-scale circulation features while mitigating some noise from localized weather variability.

(iv) Land Surface Data

To assess surface conditions, local volumetric soil water (top one-meter) was included from ERA5-Land (Muñoz-Sabater et al. 2021). This is calculated as a weighted average by depth of the top three soil layers (0-7 cm, 7-28cm, 28-100 cm) included in ERA5 land. Inclusion of this feature provides some crucial insight into land-atmosphere interactions relevant to extreme heat events, especially as climate change drives changes in land-atmosphere coupling (Qing et al. 2023).

(v) Prediction with Multiple Leads

Variables were classified as either "fast-changing" or "slow-changing." For fast-changing variables, three different leads were prescribed:

1. 21–23 days before prediction
2. 24–27 days before prediction
3. 28–34 days before prediction

For slow-changing variables, such as sea surface temperatures, certain global climate oscillations, and regional soil moisture, only one lead was used, covering 21–34 days prior to prediction. Only variables with assigned leads were included in the prediction models, except for climatology, where values for the specific prediction day were provided. A full summary of predictive variables and their lead classification is shown in Table 1.

Variable Name	Variable Type	Leads	Data Source

Max.Temp.	Meteorological	Fast-changing	ERA5-Land (Muñoz-Sabater et al. 2021)
Min. Temp.			
Relative Humidity			
10-m U-Component of Wind			
10-m V-Component of Wind			
Total Precip.			
Normal Max. Temp.	Climatology	None	
Arctic Oscillation Index	Global Climate Variability	Slow-changing	Daily Nino 3.4 Index (Derived from ERA5 Post-Processed Daily Statistics (European Centre for Medium-Range Weather Forecasts (ECMWF))
North Atlantic Oscillation Index			Daily NAO Index (Kalnay et al. 1996)
Madden-Julian Oscillation Index (Amplitude & Phase)		Fast-changing	Real-time Multivariate MJO Index (Wheeler and Hendon 2004)
Nino 3.4 Region SST	Ocean	Slow-changing	ERA5 Post-Processed Daily Statistics
Gulf of Mexico SST			
California Current SST			
300 hPa U-Component of Wind	Atmosphere	Fast-changing	ERA5 hourly single pressure level data (Hersbach et al. 2023)
300 hPa V-Component of Wind			
300 hPa Potential Vorticity			
500 hPa Geopotential Height			
Local Soil Moisture (Top one-meter)	Land Surface	Slow-changing	ERA5-Land Derived (Muñoz-Sabater et al. 2021)

Table 1. Summary of predictive variables, including their classification, lead times, and data sources.

(vi) Heat Wave Identification

In this study, heat waves were identified using a categorical approach based on daily maximum temperatures. A day was classified as a high-temperature day if its maximum temperature exceeded the 90th percentile of the daily maximum climatology. To qualify as a heat wave event, these high-temperature days were required to occur in clusters of at least three consecutive days (example shown in Figure 2). All days belonging to heat wave events were categorized as heat wave days. This threshold-based methodology ensures that the identified heat waves represent periods of sustained thermal extremes rather than isolated high-temperature occurrences. By focusing on consecutive days, the method effectively captures the persistence of heat stress that is critical for understanding its impacts on human health and ecological systems. This identification protocol provided a systematic framework for quantifying heat wave characteristics and supports the machine learning-based analysis of the strongest heat wave predictors for these cities.

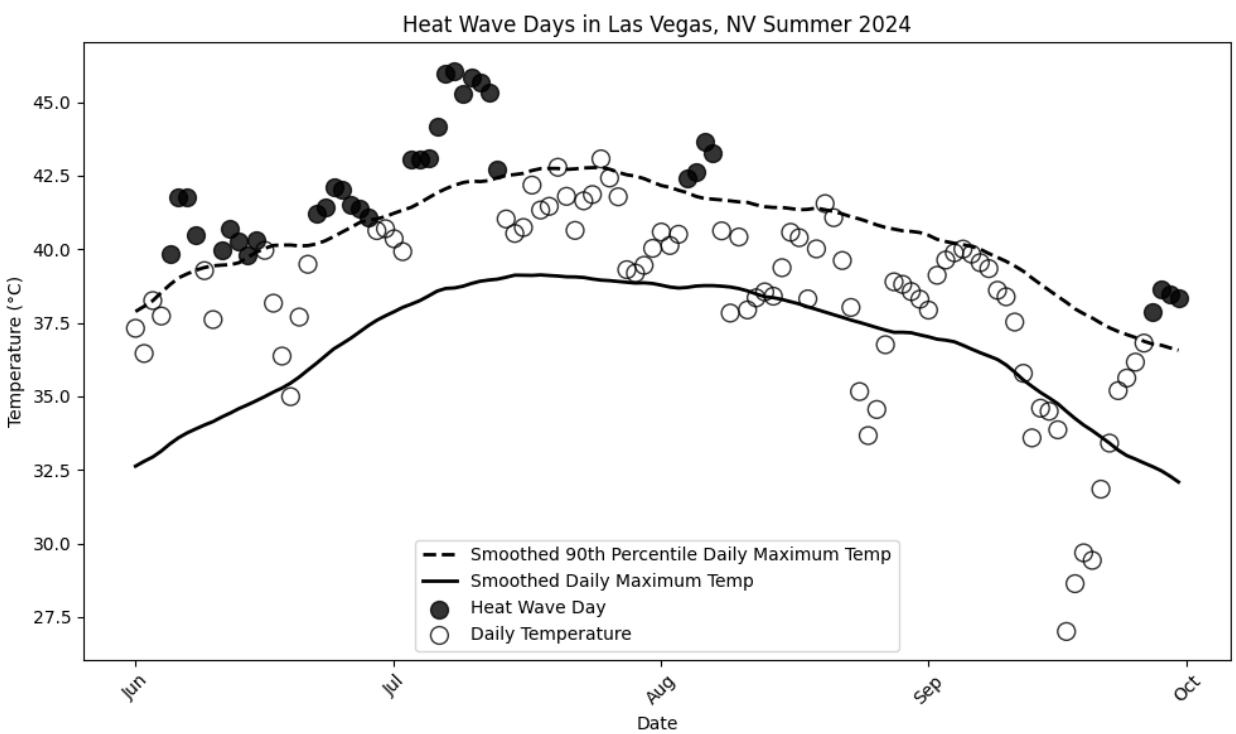

Figure 2. Example heat wave identification in Las Vegas, NV during the 2024 heat wave season as defined in this study. Curves represent smoothed daily maximum temperature climatology using a two-week running average. Individual points represent daily maximum temperatures.

Table 2 summarizes the frequency and duration of heat wave events across the six cities for the decades spanning from 1980 to 2024, during the months of June through September. Overall, 657 heat wave events totaling 3,514 days were recorded, accounting for 10.6% of the total days in the study period. Across all cities, the total number of heat wave events consistently increased each decade, from 91 events in the 1980s to 201 events in the 2010s. Correspondingly, the number of heat wave days increased significantly from 447 in the 1980s to 1,078 in the 2010s.

Dallas recorded the highest number of heat wave days (667 days) and tied with Austin for the highest number of heat wave events (117 each) over the full study period. Austin and Dallas also had the longest mean heat wave durations overall (5.7 days), while Phoenix exhibited the shortest mean duration (4.5 days). In the most recent incomplete decade (2020–2024), the frequency of heat wave events has remained high across all cities, with a total of 136 events and 886 heat wave days, suggesting a sustained elevation of heat wave occurrences into the current decade.

		Austin	**Dallas**	**Houston**	**Las Vegas**	**Mexico City**	**Phoenix**	**Total**
1980 - 1989	*Events*	9	18	14	15	14	21	**91**
	Days	55	93	79	70	74	76	**447**
1990 - 1999	*Events*	20	17	12	21	15	16	**101**
	Days	94	89	66	93	66	89	**497**
2000 - 2009	*Events*	24	22	21	24	15	22	**128**
	Days	121	110	119	109	62	85	**606**
2010 - 2019	*Events*	38	41	29	33	32	28	**201**
	Days	218	240	185	159	151	125	**1078**
2020 - 2024	*Events*	26	19	16	26	24	25	**136**
	Days	175	235	127	165	157	127	**886**
Total	*Events*	**117**	**117**	**92**	**119**	**100**	**112**	**657**
	Days	**663**	**667**	**577**	**595**	**510**	**502**	**3514**
	Mean Duration	**5.7**	**5.7**	**6.3**	**4.9**	**5.1**	**4.5**	**5.3**

Table 2. Descriptive statistics of heat wave days and events by decade in study site cities during the months of June through September.

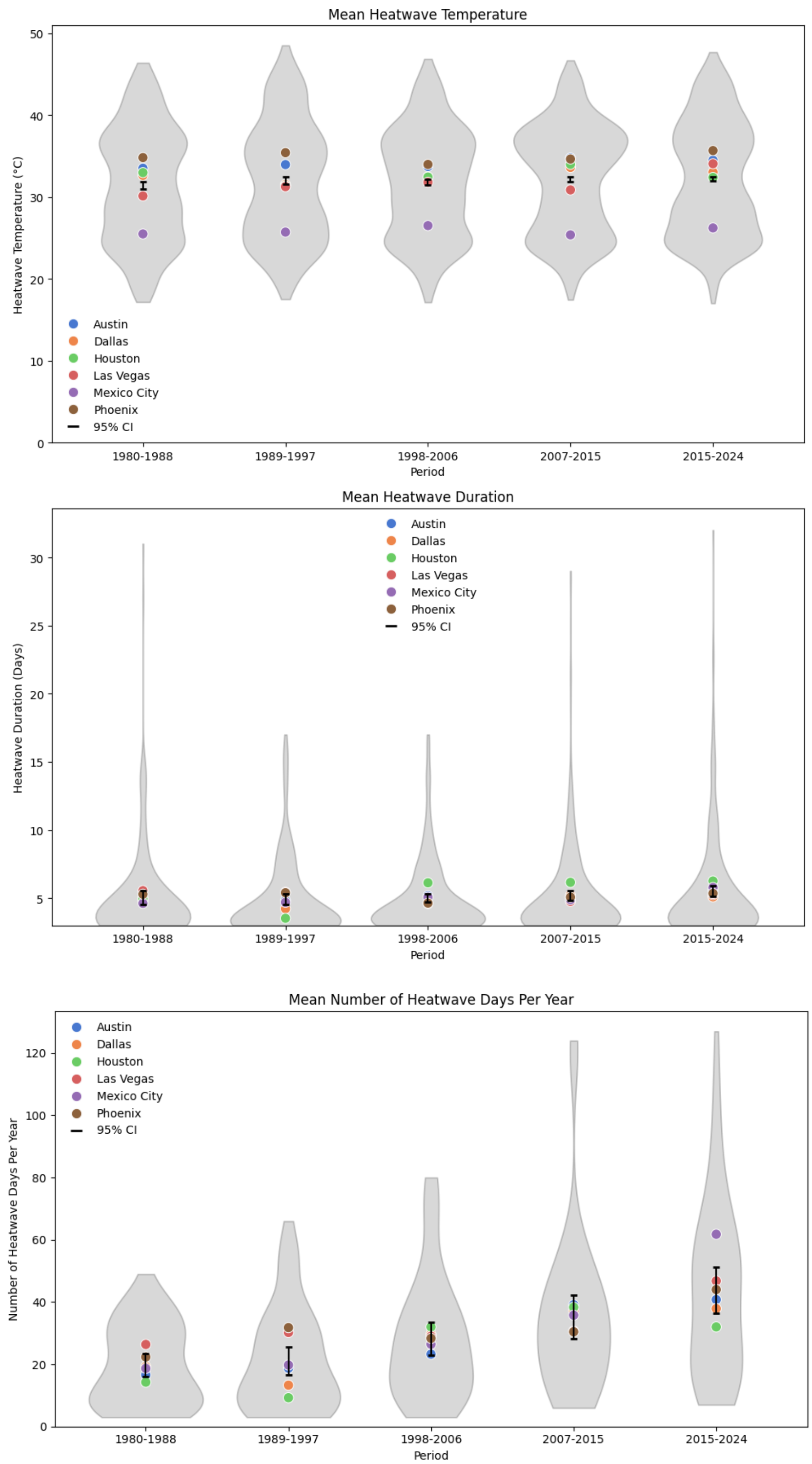

Figure 3. Violin plots of the mean heat wave temperature, heat wave duration, and number of heat wave days across all cities included in the study. Individual points mark the mean value for a city over each while 95% confidence intervals are provided for the true mean across all cities.

Figure 3 confirms changes in the number of heat wave days, illustrating changes in heat wave temperature, duration, and the number of heat wave days per year by dividing the 45-year study period into five evenly distributed 9-year periods. These plots indicate that while the mean temperature and duration of heat waves have not significantly changed across the five periods for all cities, there has been a notable increase in the mean number of heat wave days and events per year, particularly in recent periods. Furthermore, heat wave characteristics vary notably by location, with Mexico City, MX experiencing the coolest mean temperatures and Phoenix, AZ the warmest.

b. Prediction & Interpretation

Machine learning models for heat wave-day classification were developed using eXtreme Gradient Boosting (XGBoost) (Chen and Guestrin 2016), chosen for its efficiency and high performance in handling diverse input variables in classification tasks. XGBoost models were run through Scikit-learn package v1.5.2 (Pedregosa et al. 2011) in Python v3.12.6. Each variable listed in Table 1 was used to predict whether a day meets the heat-wave day criteria in a binary classification task with logistic regression as the output function, evaluated by the log loss metric.

To ensure robust model performance without overfitting, four-fold validation was used. For this, the dataset corresponding to each city was randomly divided into four subsets. In each iteration, the model was trained on three of the four subsets and tested on the remaining subset. This process was repeated to create a single ensemble model with predictive guidance based on the mean outcomes from the validation folds.

The complete four-fold validation process was repeated ten times, producing an ensemble of models. Performance metrics, including accuracy, precision, recall, and F1 score were aggregated across all ensemble members to derive mean performance values. The probability thresholds for heat wave prediction varied for each fold and were calculated to maximize F1 score. Model performance was also evaluated using the area under the precision-recall curve (PR AUC), generated for each city's XGBoost model individually. The PR AUC metric was calculated using the Scikit-learn package (Pedregosa et al. 2011) to allow for direct comparison of each city's model performance against a baseline (the proportion of heat wave days in the city’s overall dataset), providing a robust evaluation measure particularly suitable for imbalanced datasets such as heat wave occurrences.

All models were created using common parameters. The learning rate (η) was set to 0.1, and the maximum tree depth was set to 4. The fraction of rows sampled by each tree was 0.8, and the fraction of features sampled by each tree was also 0.8. To address class imbalance, a unique weighting was applied based on the relative frequency of heat wave days in each city. The weight for heat wave days (w_1) was calculated as follows:

$$w_1 = \frac{N_1}{N - N_1}$$

where N is the total number of days in the sample size, and N_1 is the total number of non-heat wave days in the dataset. This weighting scheme ensures that heat wave events, which are less frequent, contribute more significantly to the model's learning process, preventing bias toward non-heat wave days.

To interpret the contributions of each feature in the machine learning model, Shapley Additive exPlanations (SHAP) values were utilized (Lundberg and Lee 2017). SHAP values quantify each variable’s impact on model output, providing a clear interpretation of feature influence on heat-wave day classification. These values are derived by evaluating the average marginal contribution of each feature to the model's predictions. By assigning an importance score to each feature based on its contribution, the relative predictive strength of features influencing heat-wave days at a sub-seasonal time scale can be quantified. SHAP values were averaged across the ten models in the ensemble to produce mean absolute SHAP scores for each feature, as well as ensemble-based partial dependence plots, which display SHAP values as a function of feature value. SHAP values were also normalized to allow inter-model comparison, scaling each mean absolute SHAP values of each individual feature by the sum of mean absolute SHAP values for each feature included in a model.

While some features in this analysis, particularly lagged meteorological and atmospheric variables, exhibit collinearity, this primarily reduces model performance by distributing importance among related features rather than concentrating it within fewer variables. However, removing these collinear features or employing dimensionality reduction would compromise interpretability. Therefore, the presence of collinear features remains a limitation of this analysis, and caution should be exercised when interpreting results for these features, referencing Supplemental Figure 1 for context.

A final case study of a particular Las Vegas heat wave in July 2024 was analyzed to demonstrate the ability of this methodology to interpret predictors of a specific heat wave event. Conditions from 7 July 2024, a day when Las Vegas experienced a record high daily maximum temperature of 48.8 °C (National Weather Service 2024), were pushed into the ensemble XGBoost model, trained over the entire 45-year period of data from Las Vegas, to predict the probability of a heat wave given those conditions according to the model prediction. The resulting probability of a heat wave day for these conditions is then outputted, and a SHAP explainer plot is generated showing the relative contribution of each feature to this prediction.

3. Results and discussion

a. Model Skill

Overall, the XGBoost models exhibited high accuracy across all locations, ranging from 0.903 in Las Vegas and Phoenix to 0.942 in Houston (Figure 4). However, because heat wave events were relatively rare (an imbalanced class problem), other metrics such as recall, precision, and F1 score are equally important in assessing model performance. Houston achieved the highest precision and F1 score (0.574 and 0.579, respectively), while Las Vegas and Phoenix had slightly lower F1 scores, indicating slightly more difficulty in predicting heat waves in these more arid, desert climates. The confusion matrices show that across all models and cities, about 41–42.5% of true heat wave days were identified as false negatives when models were optimized for F1 score—highlighting model limitations.

Figure 4. Map of heat wave prediction metrics with representations of their mean confusion matrices, accuracy and uncertainty, and performance over baseline (as reported by PR AUC) for each city-specific XGBoost model ensemble. Prediction evaluations correspond to ensembles of ten XGBoost model ensembles each with four-fold cross validation. Error bars represent the 95% confidence intervals for the true means across the ensemble.

In addition to standard classification metrics, the study evaluated model skill via Precision-Recall Area Under the Curve (PR AUC) (Table 4). The baseline PR AUC values for each city corresponded to “random” predictions based on class imbalance alone. Houston again exhibited the strongest model performance (mean PR AUC = 0.587), substantially exceeding its baseline (0.067) and thus demonstrating reliable precision-recall tradeoffs. These PR AUC findings reinforce the importance of examining multiple metrics beyond accuracy for imbalanced predictions and demonstrate that the XGBoost models show clear skill in predicting heat waves at three-week lead times over the historical reanalysis datasets for each of the chosen cities.

b. Model interpretation

To better understand the classification methods behind the model predictions, the mean absolute SHAP scores offer insight into how various land-surface, meteorological, atmospheric, and climate predictors drive heat wave forecasts. Mean absolute SHAP values measure the overall influence of each feature on the final prediction. Several ocean features—the California Current SST, Nino 3.4 Region SST, and Gulf of Mexico SST—emerge with notably high average impact across the cities studied (Figure 5), highlighting the role of broader oceanic backgrounds. Oceanic features appear to be especially region specific, with the California Current SSTs most strongly influencing heat wave predictions for the USA cities. Soil moisture also registers high SHAP values in multiple cities, underlining the importance of land-atmosphere feedback, especially in Austin, TX and Dallas, TX. By contrast, day-to-day meteorological and atmospheric factors—such as minimum and maximum temperature, wind components, and potential vorticity at certain lags—exhibit more moderate SHAP values on average, though their influence can vary considerably depending on the location.

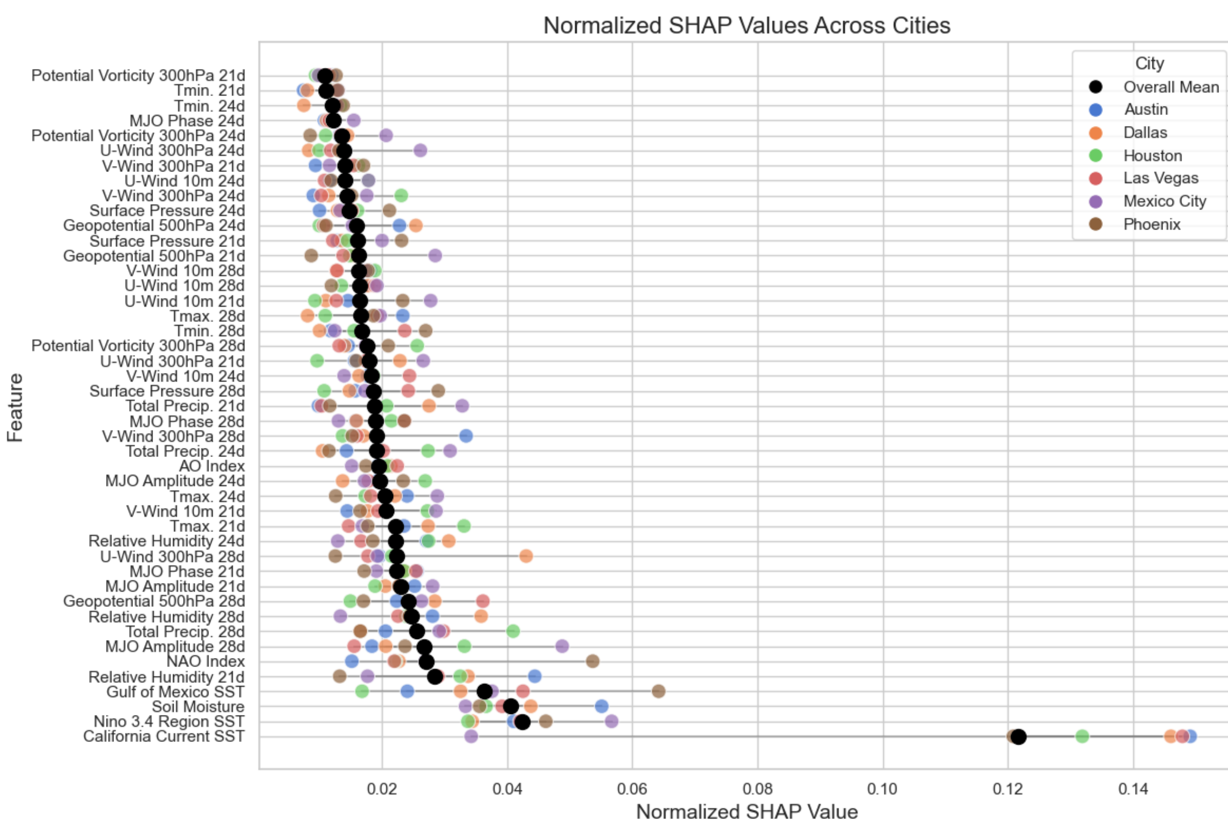

Figure 5. Normalized mean absolute SHAP values for land surface soil moisture, meteorological, atmospheric, and climate features, as averaged across the ensemble of XGBoost models trained for heat wave prediction for the chosen cities.

Partial dependence plots (Figure 6) reinforce these findings by illustrating how changes in key predictors—such as soil moisture or SST anomalies—shift the probability of a heat wave, underscoring the interplay between broader climatic conditions and local atmospheric triggers. When analyzing the partial dependence of individual features, higher SHAP values for a feature measurement indicate predictions favoring heat waves, while negative SHAP values suggest predictions against heat waves.

Examining the most influential features, all cities' models are less likely to predict heat wave events when soil moisture is higher, although the drier cities, Las Vegas and Phoenix, exhibit this trend less strongly than the other sites. Meanwhile, models for the USA cities indicate higher probabilities of heat waves during moderate Nino 3.4 region SSTs (El Niño-like conditions), whereas Mexico City's model shows the opposite tendency. Warm California Current SSTs again appear as a key driver for the US cities but exert less influence on Mexico City's predictions. Models for all cities predict higher probabilities of heat waves for the warmest Gulf of Mexico SSTs.

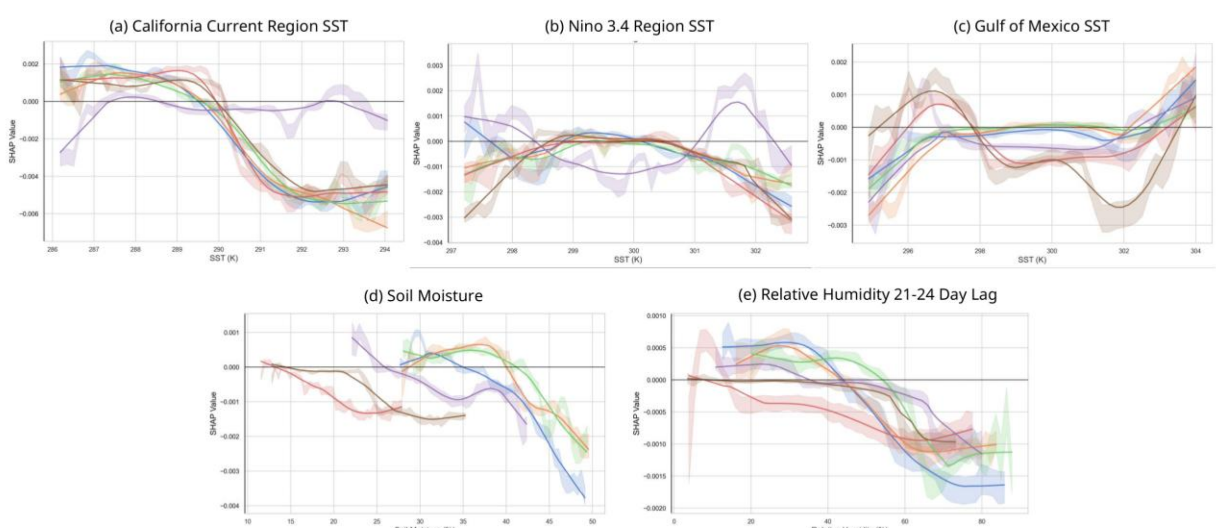

Figure 6. Scaled and normalized SHAP value plots for strong performing features. Each feature represents the average value 21-to-34 days prior to prediction unless otherwise indicated. SHAP

plots are scaled for each individual city by a constant factor according to the feature's relative SHAP score across all models trained for that city.

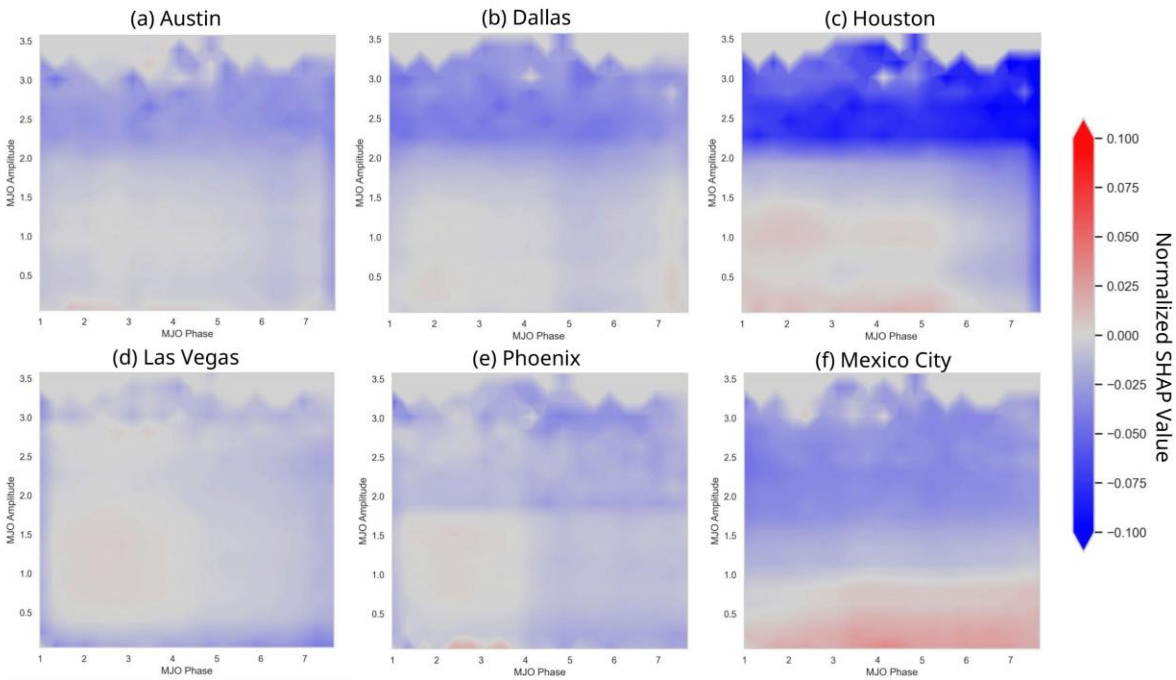

Figure 7. Bivariate partial dependence plots of MJO phase and amplitude averaged over 28-to-34-day lead time prior to heat wave prediction. Plots are scaled by a constant factor according to the sum of the relative SHAP values of both the phase and amplitude features for all models trained for each individual city.

Because the state of the MJO is characterized by both phase and amplitude, bivariate partial dependence plots (Figure 7) show how these two parameters modulate heat wave probabilities in model predictions over a 28–34-day lead. In Mexico City, there is a consistent inverse relationship between MJO amplitude and heat wave prediction probability. For the cities in the United States, prediction of a heat wave at four weeks lead time is more likely when the MJO is in phases one through four and at lower amplitudes, and less likely at higher amplitudes and/or later phases.

c. Application to single-heat wave events

On July 7, 2024—the hottest day on record for Las Vegas with temperatures rising over 48.5 °C (National Weather Service 2024)—the ensemble model predicted a 97.2% chance of a heat wave, with a 95% confidence interval ranging from 96.6% to 97.9%. Figure 8 illustrates the most influential feature contributions (as determined by SHAP values) for this specific event. Positive contributions (red) increase the likelihood of a heat wave, while negative contributions (blue) reduce it. Notably, MJO Amplitude at a 24-day lead, elevated surface pressure at that same lag, and recent temperature anomalies all push prediction towards a heat wave event, whereas certain geopotential height anomalies and longer-lead precipitation features reduce strength of that prediction. These interactions highlight the complex interplay among multiple atmospheric variables; heat waves require the alignment of multiple climate drivers, and this model can be applied to form insights regarding the specific combinations of those drivers as they interact in individual events.

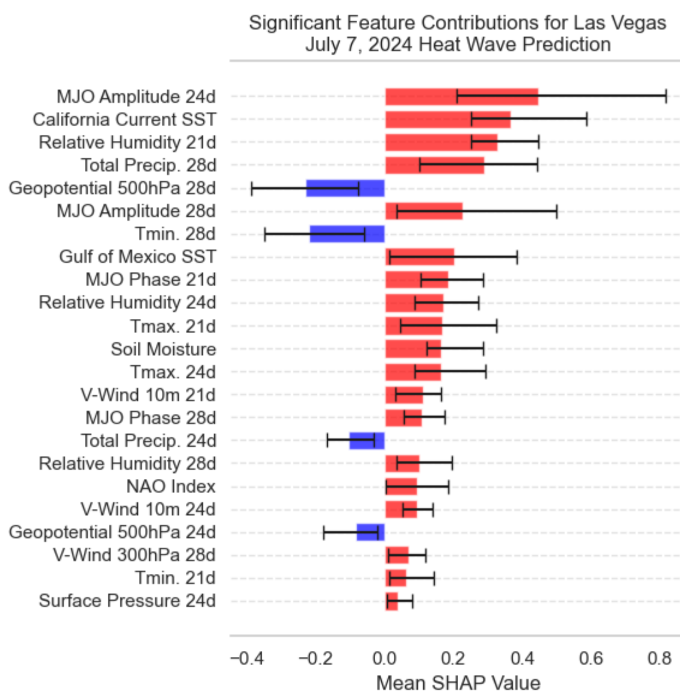

Figure 8. SHAP values derived from ensemble model predictions using conditions from the 7 July 2024 heat wave day in Las Vegas. Error bars represent the 95% confidence interval for the true mean SHAP value across the ensemble.

These results suggest that sea surface temperatures, followed by land-surface soil moisture, emerge as the strongest sub-seasonal predictors of heat waves for the Northern Hemisphere cities examined. More broadly, the current theoretical understanding of global climate dynamics posits that three-week temperature predictability largely originates from land-surface processes, which retain memory over weeks to months; by this time range, the influence of initial atmospheric conditions has substantially diminished, and initial oceanic temperatures are not yet exerting a significant effect. Additionally, predictability arises from global climate oscillation, including the ENSO, the MJO, and NAO (DelSole et al. 2017). However, recent studies using the CESM2 model indicate that mid-latitude three-week temperature predictability may derive nearly equally from oceanic and atmospheric processes, as well as from land-atmosphere feedbacks (Richter et al. 2024). This varies for the mid-latitudes, where atmospheric processes may exhibit greater influence. The findings here corroborate Richter et al.'s findings in countering the conventional hypotheses behind sub-seasonal three-week lead time predictability, showing that longer-term ocean, atmospheric, and global climate processes all show predictive signals at three-week lead times. An earlier study by Wehrli et al. found that atmospheric and land surface processes are key to the formation of heat waves through CESM analysis, with oceanic processes not contributing significantly to their formation (2019). These results counter that study, suggesting that for extreme heat events, the proper combination of background climate conditions is essential for the formation and persistence of sustained heat waves (Miralles et al. 2012). Additionally, these results provide nuance to the highly region-specific influence of certain climate drivers on this time scale.

These model predictions gain further validity by aligning, in most cases, with well-established physical mechanisms. In particular, the partial dependence plot for soil moisture in the Texas Gulf Coast region corroborates previous research, showing that positive soil moisture anomalies generally correspond to a lower likelihood of heat-wave days. Benson and Dirmeyer (2021) reported a strong negative correlation ($r < -0.7$) between daily soil moisture and maximum temperature in this region, although they also noted the non-linear regime dependent nature of this relationship (weakly-coupled, sensitive, and hypersensitive). This study provides strong evidence that, below the mean soil moisture threshold, heat extremes are more likely, marking the transition between the sensitive and hypersensitive regime. Below the mean soil moisture threshold, our analysis indicates a marked increase in heat extremes, signaling a shift from the sensitive to the hypersensitive regime. Dynamic modeling further supports the critical role of soil moisture in heat-wave formation for climates situated between humid and arid conditions (Seo et al. 2019), which helps explain why local soil moisture appears especially predictive of heat waves in Austin, TX and Dallas, TX compared with other cities examined.

SSTs exhibit particularly interesting dynamics, with warm Niño 3.4 Region SSTs and Gulf of Mexico SSTs both showing strong predictive influence on heat waves in all modeled cities except Mexico City. Warmer SSTs can induce near-surface convergence, which promotes upward motion and potential cloud formation (Minobe et al. 2008). These processes also highlight important teleconnections on multiple spatiotemporal scales (Small et al. 2023). However, Mexico City's more tropical latitude, as well as high elevation and unique plateau setting appear to reduce the relative impact of these remote SST signals, leading heat wave prediction to be more dependent on localized atmospheric conditions than on large-scale oceanic patterns.

Despite these promising insights, fully separating individual processes without losing key information remains difficult. For instance, while the model demonstrates that the MJO contributes region-dependent skill at various lead times, considering both its phase and amplitude, it is plausible that some of the MJO's predictive power is masked by correlations with other climate features utilized in this study (notably, Pacific SSTs). Given the relationships between the MJO and other oscillations, such as ENSO (Arcodia et al. 2020) and the QBO (Mundhenk et al. 2018), further co-analyses are warranted to isolate their independent effects.

Additionally, other atmospheric processes not included in this study may hold significant value for improving heat wave prediction. These include identifiable features such as quasi-stationary Rossby waves (Schubert et al. 2011) and atmospheric rivers (Scholz and Lora 2024). Although the present model has not explicitly accounted for these larger-scale dynamics, incorporating them into future model developments could provide deeper insight into heat wave onset mechanisms. By broadening the scope of predictors, further development with this method can continue refining sub-seasonal forecasting techniques and better capture complex interplays between multiple climate drivers.

Although these predictive models have been optimized to balance false positives and false negatives, they can be intentionally adjusted to minimize false negatives—choosing to over-predict potential heat waves rather than risk missing true events. However, for reasons related to both data availability as well as the lack robust training and testing splits designed to handle non-stationarity, the method is not currently recommended for any operational prediction. Specifically, the evolving long-term trends in heat waves due to climate change indicate that historical predictors may lose some reliability over longer training periods. While the model can be applied to regions beyond North America, caution is advised in areas that assimilate fewer data points into reanalysis datasets. Therefore, the use of this method for operational forecasting is strongly discouraged in its present state; rather, value should be taken in these results for an understanding of the predictors of heat waves over the sub-seasonal time scale for these North American cities.

4. Conclusions

XGBoost models trained on a diverse set of climate drivers demonstrate skill in predicting past heat waves at a 21-day lead time in North America, with key region-specific sea surface temperatures and soil moisture emerging as the strongest common predictors. While overall predictive skill is consistent across study sites, the relative importance of these predictors varies significantly, offering valuable insights into the unique local climate dynamics of each area. This study establishes a crucial foundation for addressing inherent limitations in sub-seasonal forecasting and paves the way for the development of regional hybrid models that integrate machine-learning and dynamical approaches—an approach that holds promise for localized heat-health impact predictions. With further refinement into an operational prediction product, this methodology could lead to critical improvements in public health preparedness, particularly in urban centers increasingly vulnerable to heat wave risks.

Future work will test these predictions in real time and continuously update the training sets, acknowledging that evolving heat-wave dynamics under climate change may shift predictor trends and their relative importance. Moreover, integrating dynamical sub-seasonal models with machine-learning methods is essential for enhancing predictions of extreme heat events, especially when conditions fall outside historical norms.

Acknowledgements

J.J.A. acknowledges the University of Texas at Austin, Jackson School of Geosciences, Department of Earth and Planetary Sciences, for support through a Graduate Fellowship, Graduate Teaching Assistantship, and Independent Study Semester Fellowship. Additionally, we extend our gratitude to Geeta G. Persad, Danielle Touma, Zoltan Sylvester, and Catherine Cubbin for their valuable insights, which helped guide this study.

Data Availability Statement

The datasets analyzed in this study are publicly available from multiple sources. ERA5 post-processed daily statistics data were retrieved using the Climate Data Store API (CDS API; https://cds.climate.copernicus.eu/). ERA5-Land daily data were accessed and post-processed via Google Earth Engine (https://earthengine.google.com/). Daily North Atlantic Oscillation (NAO) and Arctic Oscillation (AO) indices were obtained from the NOAA Climate Prediction Center (https://www.cpc.ncep.noaa.gov/). The Madden-Julian Oscillation (MJO) Real-time Multivariate MJO (RMM) indices are available from the Australian Bureau of Meteorology (http://www.bom.gov.au/climate/mjo/).

REFERENCES

Aquino-Martínez, L. P., B. Ortega-Guerrero, A. I. Quintanar, and Y. Díaz-Esteban, 2025: Synoptic patterns and heatwaves: Intensifying urban heat islands in the Mexico Basin. *Urban Climate*, **59**, 102318, https://doi.org/10.1016/j.uclim.2025.102318.

Arcodia, M. C., B. P. Kirtman, and L. S. P. Siqueira, 2020: How MJO Teleconnections and ENSO Interference Impacts U.S. Precipitation, https://doi.org/10.1175/JCLI-D-19-0448.1.

Benson, D. O., and P. A. Dirmeyer, 2021: Characterizing the Relationship between Temperature and Soil Moisture Extremes and Their Role in the Exacerbation of Heat Waves over the Contiguous United States, https://doi.org/10.1175/JCLI-D-20-0440.1.

Boumans, R. J. M., D. L. Phillips, W. Victery, and T. D. Fontaine, 2014: Developing a model for effects of climate change on human health and health–environment interactions: Heat stress in Austin, Texas. *Urban Climate*, **8**, 78–99, https://doi.org/10.1016/j.uclim.2014.03.001.

Chen, T., and C. Guestrin, 2016: XGBoost: A Scalable Tree Boosting System. *Proceedings of the 22nd ACM SIGKDD International Conference on Knowledge Discovery and Data Mining*, *KDD '16*, New York, NY, USA, Association for Computing Machinery, 785–794, https://doi.org/10.1145/2939672.2939785.

Chung, U., J. Rhee, M. Kim, and S.-J. Sohn, 2024: Advancing sub-seasonal to seasonal multi-model ensemble precipitation prediction in east asia: Deep learning-based post-processing for improved accuracy. *Heliyon*, **10**, https://doi.org/10.1016/j.heliyon.2024.e35933.

DelSole, T., L. Trenary, M. K. Tippett, and K. Pegion, 2017: Predictability of Week-3–4 Average Temperature and Precipitation over the Contiguous United States, https://doi.org/10.1175/JCLI-D-16-0567.1.

European Centre for Medium-Range Weather Forecasts (ECMWF),: ERA5 post-processed daily statistics on pressure levels from 1940 to present. Copernicus Climate Change Service (C3S) Climate Data Store (CDS), accessed 3 March 2025, https://doi.org/10.24381/cds.50314f4c.

Habeeb, D., J. Vargo, and B. Stone, 2015: Rising heat wave trends in large US cities. *Nat Hazards*, **76**, 1651–1665, https://doi.org/10.1007/s11069-014-1563-z.

He, S., X. Li, L. Trenary, B. A. Cash, T. DelSole, and A. Banerjee, 2022: Learning and Dynamical Models for Sub-seasonal Climate Forecasting: Comparison and Collaboration. *AAAI*, **36**, 4495–4503, https://doi.org/10.1609/aaai.v36i4.20372.

Hersbach, H., and Coauthors, 2023: ERA5 hourly data on single levels from 1940 to present. Copernicus Climate Change Service (C3S) Climate Data Store (CDS), accessed 17 September 2024, https://doi.org/10.24381/CDS.ADBB2D47.

Howard, J. T., N. Androne, K. C. Alcover, and A. R. Santos-Lozada, 2024: Trends of Heat-Related Deaths in the US, 1999-2023. *JAMA*, **332**, https://doi.org/10.1001/jama.2024.16862.

Hwang, J., P. Orenstein, J. Cohen, K. Pfeiffer, and L. Mackey, 2019: Improving Subseasonal Forecasting in the Western U.S. with Machine Learning. *Proceedings of the 25th ACM SIGKDD International Conference on Knowledge Discovery & Data Mining*, *KDD '19*, New York, NY, USA, Association for Computing Machinery, 2325–2335, https://doi.org/10.1145/3292500.3330674.

Jenney, A. M., K. M. Nardi, E. A. Barnes, and D. A. Randall, 2019: The Seasonality and Regionality of MJO Impacts on North American Temperature. *Geophysical Research Letters*, **46**, 9193–9202, https://doi.org/10.1029/2019GL083950.

Jiang, L., J. Zhang, Q. Liu, X. Meng, L. Shi, D. Zhang, and M. Xing, 2023: Spatiotemporal variations of the global compound heat wave and the drivers of its spatial heterogeneity. *Journal of Cleaner Production*, **408**, 137201, https://doi.org/10.1016/j.jclepro.2023.137201.

Kalnay, E., and Coauthors, 1996: The NCEP/NCAR 40-Year Reanalysis Project.

Kimmel Jr., T. M., J. Nielsen-Gammon, B. Rose, and H. M. Mogil, 2016: The Weather and Climate of Texas: A Big State With Big Extremes. *Weatherwise*, **69**, 25–33, https://doi.org/10.1080/00431672.2016.1206446.

Lee, E., R. Bieda, J. Shanmugasundaram, and H. Basara Richter, 2016: Land surface and atmospheric conditions associated with heat waves over the Chickasaw Nation in the South Central United States. *Journal of Geophysical Research: Atmospheres*, **121**, 6284–6298, https://doi.org/10.1002/2015JD024659.

Lin, H., R. Mo, and F. Vitart, 2022: The 2021 Western North American Heatwave and Its Subseasonal Predictions. *Geophysical Research Letters*, **49**, e2021GL097036, https://doi.org/10.1029/2021GL097036.

Lowe, R., M. García-Díez, J. Ballester, J. Creswick, J.-M. Robine, F. R. Herrmann, and X. Rodó, 2016: Evaluation of an Early-Warning System for Heat Wave-Related Mortality in Europe: Implications for Sub-seasonal to Seasonal Forecasting and Climate Services. *International Journal of Environmental Research and Public Health*, **13**, 206, https://doi.org/10.3390/ijerph13020206.

Lundberg, S. M., and S.-I. Lee, 2017: A Unified Approach to Interpreting Model Predictions. *Advances in Neural Information Processing Systems*, Vol. 30 of, Curran Associates, Inc.

Luo, M., and N.-C. Lau, 2020: Summer heat extremes in northern continents linked to developing ENSO events. *Environ. Res. Lett.*, **15**, 074042, https://doi.org/10.1088/1748-9326/ab7d07.

McGregor, G., 2024: Synoptic Scale Atmospheric Processes and Heatwaves. *Heatwaves: Causes, Consequences and Responses*, G. McGregor, Ed., Springer International Publishing, 207–259, https://doi.org/10.1007/978-3-031-69906-1_6.

Miller, D. E., Z. Wang, B. Li, D. S. Harnos, and T. Ford, 2021: Skillful Subseasonal Prediction of U.S. Extreme Warm Days and Standardized Precipitation Index in Boreal Summer, https://doi.org/10.1175/JCLI-D-20-0878.1.

Miloshevich, G., B. Cozian, P. Abry, P. Borgnat, and F. Bouchet, 2023: Probabilistic forecasts of extreme heatwaves using convolutional neural networks in a regime of lack of data. *Phys. Rev. Fluids*, **8**, 040501, https://doi.org/10.1103/PhysRevFluids.8.040501.

Minobe, S., A. Kuwano-Yoshida, N. Komori, S.-P. Xie, and R. J. Small, 2008: Influence of the Gulf Stream on the troposphere. *Nature*, **452**, 206–209, https://doi.org/10.1038/nature06690.

Miralles, D. G., M. J. van den Berg, A. J. Teuling, and R. a. M. de Jeu, 2012: Soil moisture-temperature coupling: A multiscale observational analysis. *Geophysical Research Letters*, **39**, https://doi.org/10.1029/2012GL053703.

Mundhenk, B. D., E. A. Barnes, E. D. Maloney, and C. F. Baggett, 2018: Skillful empirical subseasonal prediction of landfalling atmospheric river activity using the Madden–Julian oscillation and quasi-biennial oscillation. *npj Clim Atmos Sci*, **1**, 1–7, https://doi.org/10.1038/s41612-017-0008-2.

Muñoz-Sabater, J., and Coauthors, 2021: ERA5-Land: a state-of-the-art global reanalysis dataset for land applications. *Earth System Science Data*, **13**, 4349–4383, https://doi.org/10.5194/essd-13-4349-2021.

National Weather Service, 2024: *Temperature Overview*. National Weather Service, Las Vegas Weather Forecast Office, https://www.weather.gov/media/vef/Temperature%20Overview.pdf.

NOAA Climate Prediction Center,: Daily Arctic Oscillation (AO) Index, https://www.cpc.ncep.noaa.gov/products/precip/CWlink/daily_ao_index/ao_index.html.

Parker, T. J., G. J. Berry, and M. J. Reeder, 2013: The influence of tropical cyclones on heat waves in Southeastern Australia. *Geophysical Research Letters*, **40**, 6264–6270, https://doi.org/10.1002/2013GL058257.

Pedregosa, F., and Coauthors, 2011: Scikit-learn: Machine Learning in Python. *J. Mach. Learn. Res.*, **12**, 2825–2830.

Pegion, K., and Coauthors, 2019: The Subseasonal Experiment (SubX): A Multimodel Subseasonal Prediction Experiment, https://doi.org/10.1175/BAMS-D-18-0270.1.

Perkins-Kirkpatrick, S. E., and P. B. Gibson, 2017: Changes in regional heatwave characteristics as a function of increasing global temperature. *Sci Rep*, **7**, 12256, https://doi.org/10.1038/s41598-017-12520-2.

Qing, Y., S. Wang, Z.-L. Yang, P. Gentine, B. Zhang, and J. Alexander, 2023: Accelerated soil drying linked to increasing evaporative demand in wet regions. *npj Clim Atmos Sci*, **6**, 1–10, https://doi.org/10.1038/s41612-023-00531-y.

Richardson, D., H. Cloke, and F. Pappenberger, 2020: Evaluation of the Consistency of ECMWF Ensemble Forecasts. *Geophysical Research Letters*, **47**, https://doi.org/10.1029/2020GL087934.

Richter, J. H., and Coauthors, 2024: Quantifying sources of subseasonal prediction skill in CESM2. *npj Clim Atmos Sci*, **7**, 1–9, https://doi.org/10.1038/s41612-024-00595-4.

Scholz, S. R., and J. M. Lora, 2024: Atmospheric rivers cause warm winters and extreme heat events. *Nature*, **636**, 640–646, https://doi.org/10.1038/s41586-024-08238-7.

Schubert, S., H. Wang, and M. Suarez, 2011: Warm Season Subseasonal Variability and Climate Extremes in the Northern Hemisphere: The Role of Stationary Rossby Waves, https://doi.org/10.1175/JCLI-D-10-05035.1.

Seo, E., and Coauthors, 2019: Impact of soil moisture initialization on boreal summer subseasonal forecasts: mid-latitude surface air temperature and heat wave events. *Clim Dyn*, **52**, 1695–1709, https://doi.org/10.1007/s00382-018-4221-4.

Seong, K., J. Jiao, and A. Mandalapu, 2023: Evaluating the effects of heat vulnerability on heat-related emergency medical service incidents: Lessons from Austin, Texas. *Environment and Planning B: Urban Analytics and City Science*, **50**, 776–795, https://doi.org/10.1177/23998083221129618.

Small, R. J., V. Rousseau, R. Parfitt, L. Laurindo, L. O'Neill, R. Masunaga, N. Schneider, and P. Chang, 2023: Near-Surface Wind Convergence over the Gulf Stream—The Role of SST Revisited, https://doi.org/10.1175/JCLI-D-22-0441.1.

Tuel, A., and O. Martius, 2023: Weather persistence on sub-seasonal to seasonal timescales: a methodological review. *Earth System Dynamics*, **14**, 955–987, https://doi.org/10.5194/esd-14-955-2023.

Vargas, N., and V. Magaña, 2020: Warm Spells and Climate Risk to Human Health in the Mexico City Metropolitan Area, https://doi.org/10.1175/WCAS-D-19-0096.1.

Ventura, S., J. R. Miró, J. C. Peña, and G. Villalba, 2023: Analysis of synoptic weather patterns of heatwave events. *Clim Dyn*, **61**, 4679–4702, https://doi.org/10.1007/s00382-023-06828-1.

Vitart, F., and A. W. Robertson, 2018: The sub-seasonal to seasonal prediction project (S2S) and the prediction of extreme events. *npj Clim Atmos Sci*, **1**, 1–7, https://doi.org/10.1038/s41612-018-0013-0.

Wang, W., W. Zhou, X. Li, X. Wang, and D. Wang, 2016: Synoptic-scale characteristics and atmospheric controls of summer heat waves in China. *Clim Dyn*, **46**, 2923–2941, https://doi.org/10.1007/s00382-015-2741-8.

Wehrli, K., B. Guillod, M. Hauser, M. Leclair, and S. Seneviratne, 2019: Identifying Key Driving Processes of Major Recent Heat Waves. *Journal of Geophysical Research: Atmospheres*.

Weirich-Benet, E., M. Pyrina, B. Jiménez-Esteve, E. Fraenkel, J. Cohen, and D. I. V. Domeisen, 2023: Subseasonal Prediction of Central European Summer Heatwaves with Linear and Random Forest Machine Learning Models, https://doi.org/10.1175/AIES-D-22-0038.1.

Wheeler, M. C., and H. H. Hendon, 2004: An All-Season Real-Time Multivariate MJO Index: Development of an Index for Monitoring and Prediction. *Monthly Weather Review*, **132**, 1917–1932, https://doi.org/10.1175/1520-0493(2004)132<1917:AARMMI>2.0.CO;2.

White, C. J., and Coauthors, 2022: Advances in the Application and Utility of Subseasonal-to-Seasonal Predictions, https://doi.org/10.1175/BAMS-D-20-0224.1.

Yu, B., H. Lin, R. Mo, and G. Li, 2023: A physical analysis of summertime North American heatwaves. *Clim Dyn*, **61**, 1551–1565, https://doi.org/10.1007/s00382-022-06642-1.

Zhang, X., and Coauthors, 2023: Increased impact of heat domes on 2021-like heat extremes in North America under global warming. *Nat Commun*, **14**, 1690, https://doi.org/10.1038/s41467-023-37309-y.

Supplemental Materials

Supplemental Figure 1. Collinearity matrices of all model features across the full dataset for each individual city.

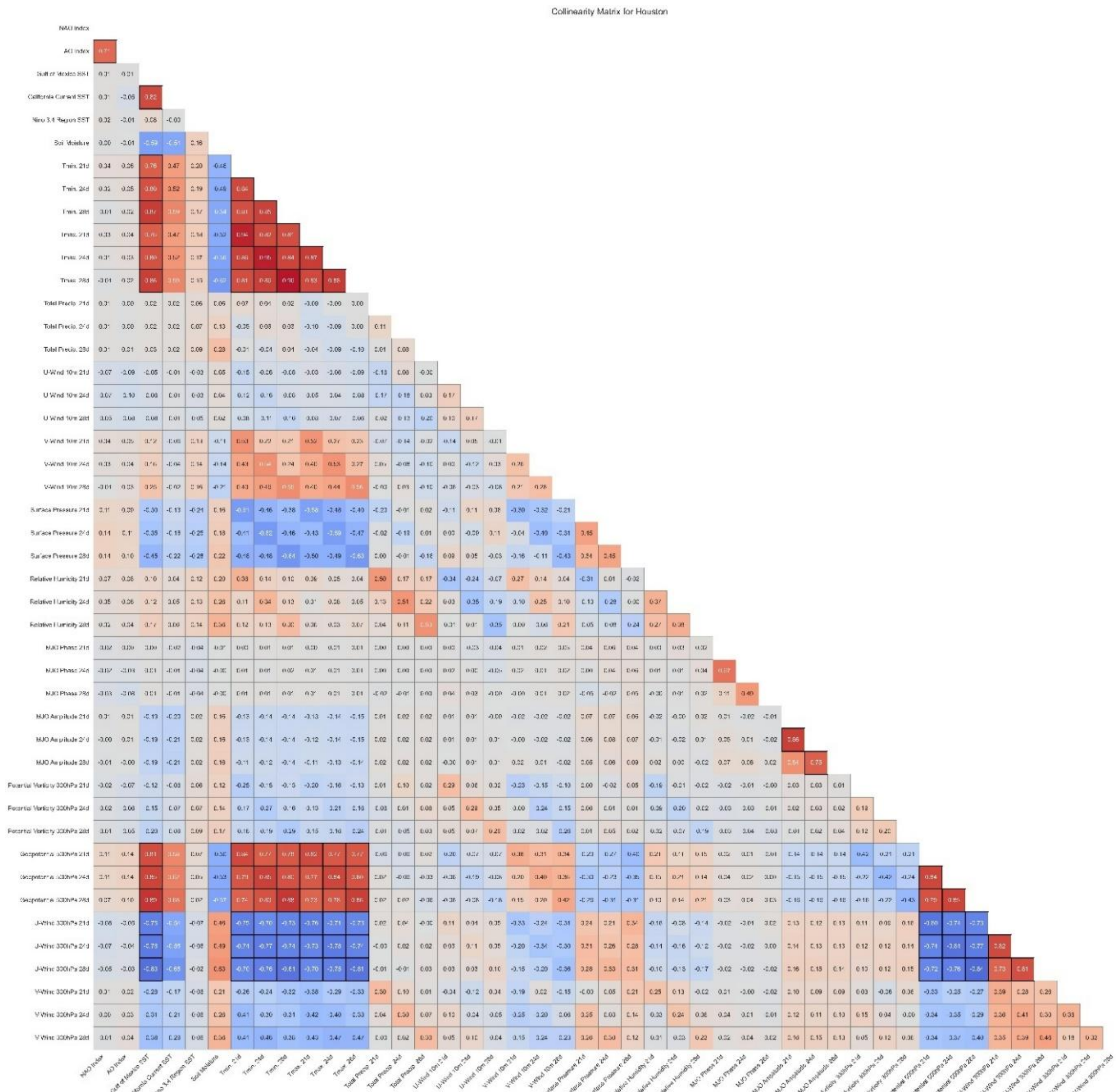

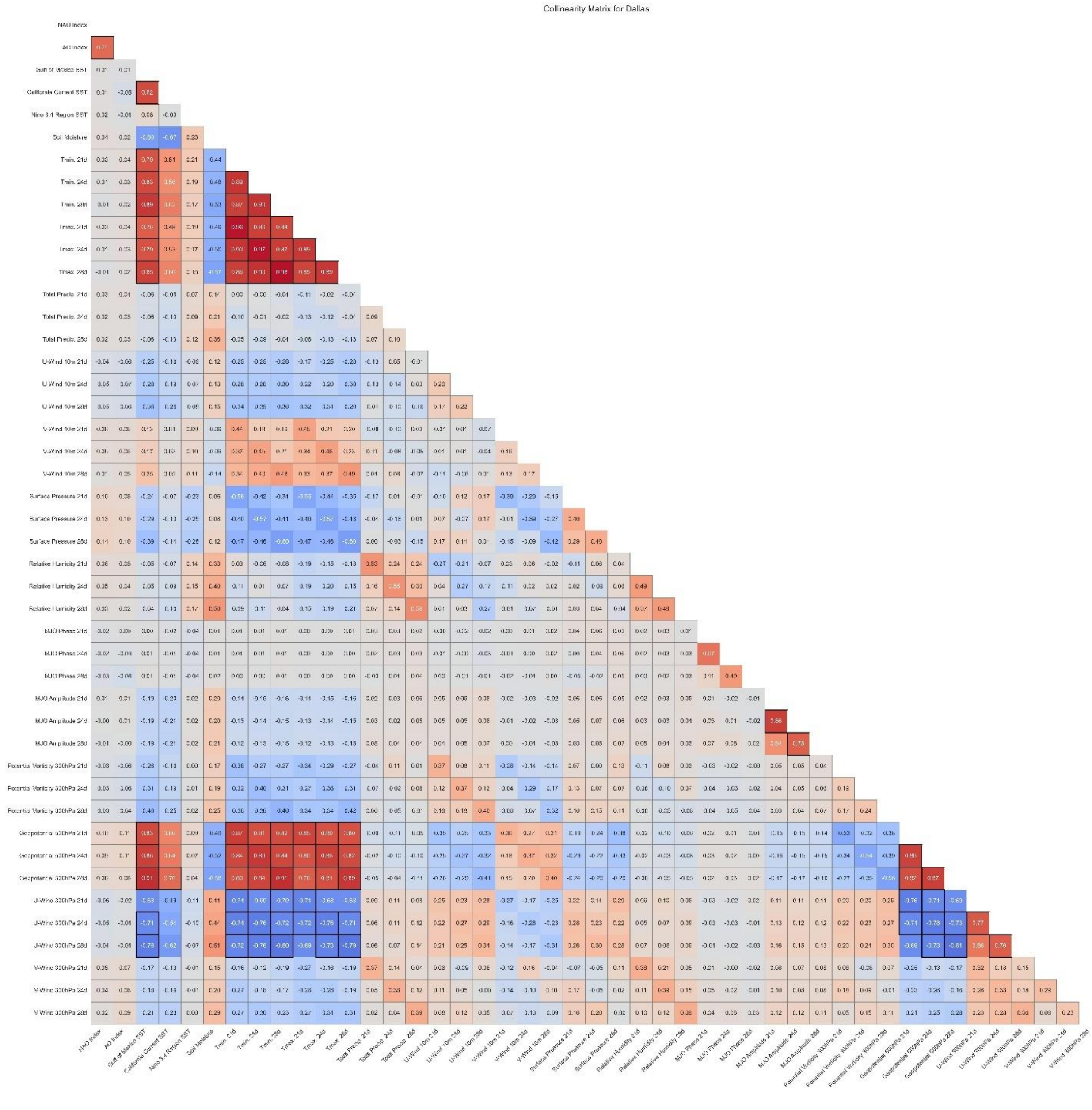

Collinearity Matrix for Dallas
NAO Index
AO Index
Gulf of Mexico SST
California Current SST
Nino 3.4 Region SST
Soil Moisture
Tmin 21d
Tmin 24d
Tmin 28d
Tmax 21d
Tmax 24d
Tmax 28d
Total Precip 21d
Total Precip 24d
Total Precip 28d
U-Wind 10m 21d
U-Wind 10m 24d
U-Wind 10m 28d
V-Wind 10m 21d
V-Wind 10m 24d
V-Wind 10m 28d
Surface Pressure 21d
Surface Pressure 24d
Surface Pressure 28d
Relative Humidity 21d
Relative Humidity 24d
Relative Humidity 28d
MJO Phase 21d
MJO Phase 24d
MJO Phase 28d
MJO Amplitude 21d
MJO Amplitude 24d
MJO Amplitude 28d
Potential Vorticity 300hPa 21d
Potential Vorticity 300hPa 24d
Potential Vorticity 300hPa 28d
Geopotential 500hPa 21d
Geopotential 500hPa 24d
Geopotential 500hPa 28d
U-Wind 300hPa 21d
U-Wind 300hPa 24d
U-Wind 300hPa 28d
V-Wind 300hPa 21d
V-Wind 300hPa 24d
V-Wind 300hPa 28d

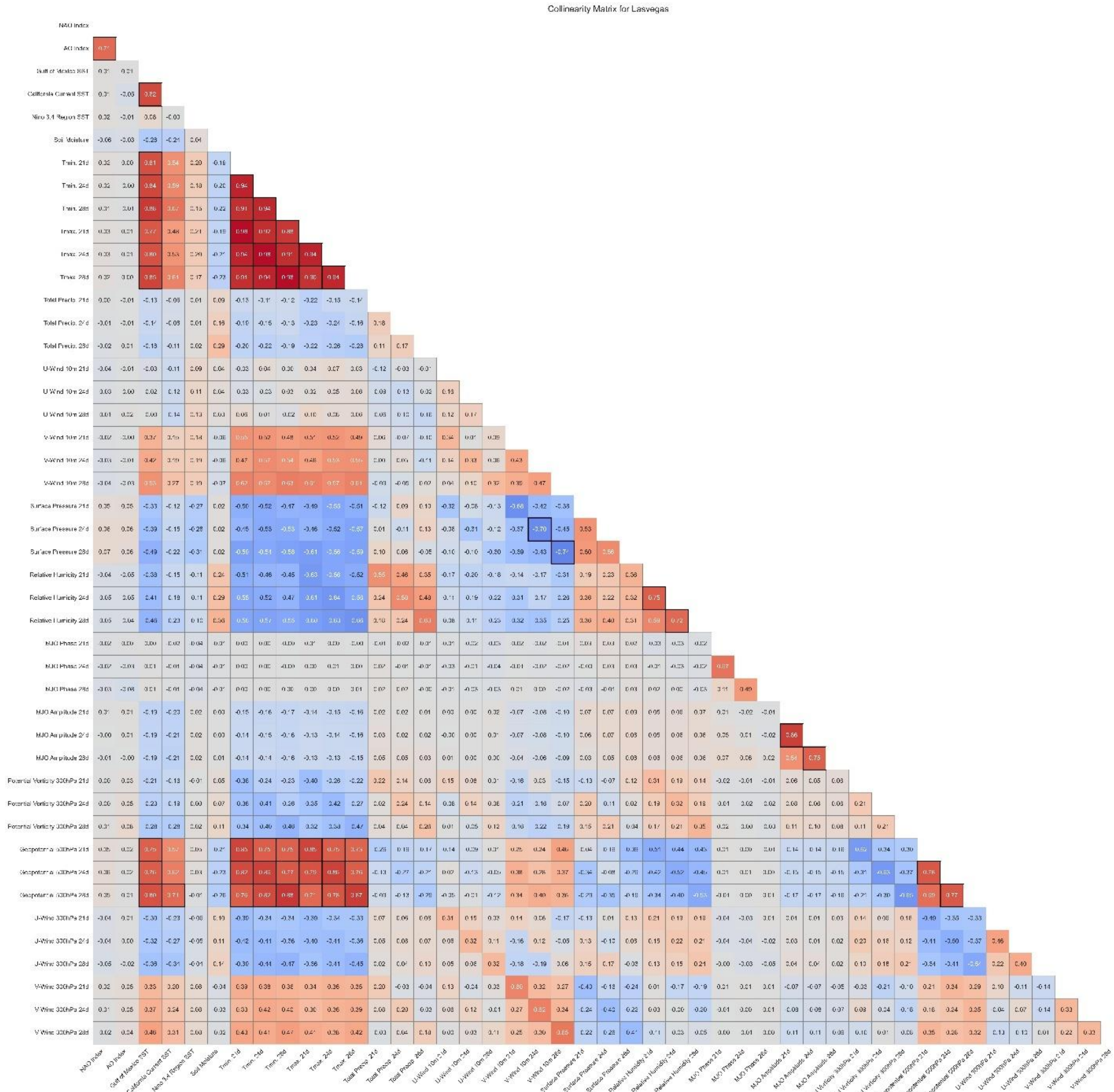

Collinearity Matrix for Lasvegas
NAO Index
AO Index
Gulf of Mexico SST
California Current SST
Nino 3.4 Region SST
Soil Moisture
Tmin 21d
Tmin 24d
Tmin 28d
Tmax 21d
Tmax 24d
Tmax 28d
Total Precip 21d
Total Precip 24d
Total Precip 28d
U-Wind 10m 21d
U-Wind 10m 24d
U-Wind 10m 28d
V-Wind 10m 21d
V-Wind 10m 24d
V-Wind 10m 28d
Surface Pressure 21d
Surface Pressure 24d
Surface Pressure 28d
Relative Humidity 21d
Relative Humidity 24d
Relative Humidity 28d
MJO Phase 21d
MJO Phase 24d
MJO Phase 28d
MJO Amplitude 21d
MJO Amplitude 24d
MJO Amplitude 28d
Potential Vorticity 300hPa 21d
Potential Vorticity 300hPa 24d
Potential Vorticity 300hPa 28d
Geopotential 500hPa 21d
Geopotential 500hPa 24d
Geopotential 500hPa 28d
U-Wind 300hPa 21d
U-Wind 300hPa 24d
U-Wind 300hPa 28d
V-Wind 300hPa 21d
V-Wind 300hPa 24d
V-Wind 300hPa 28d

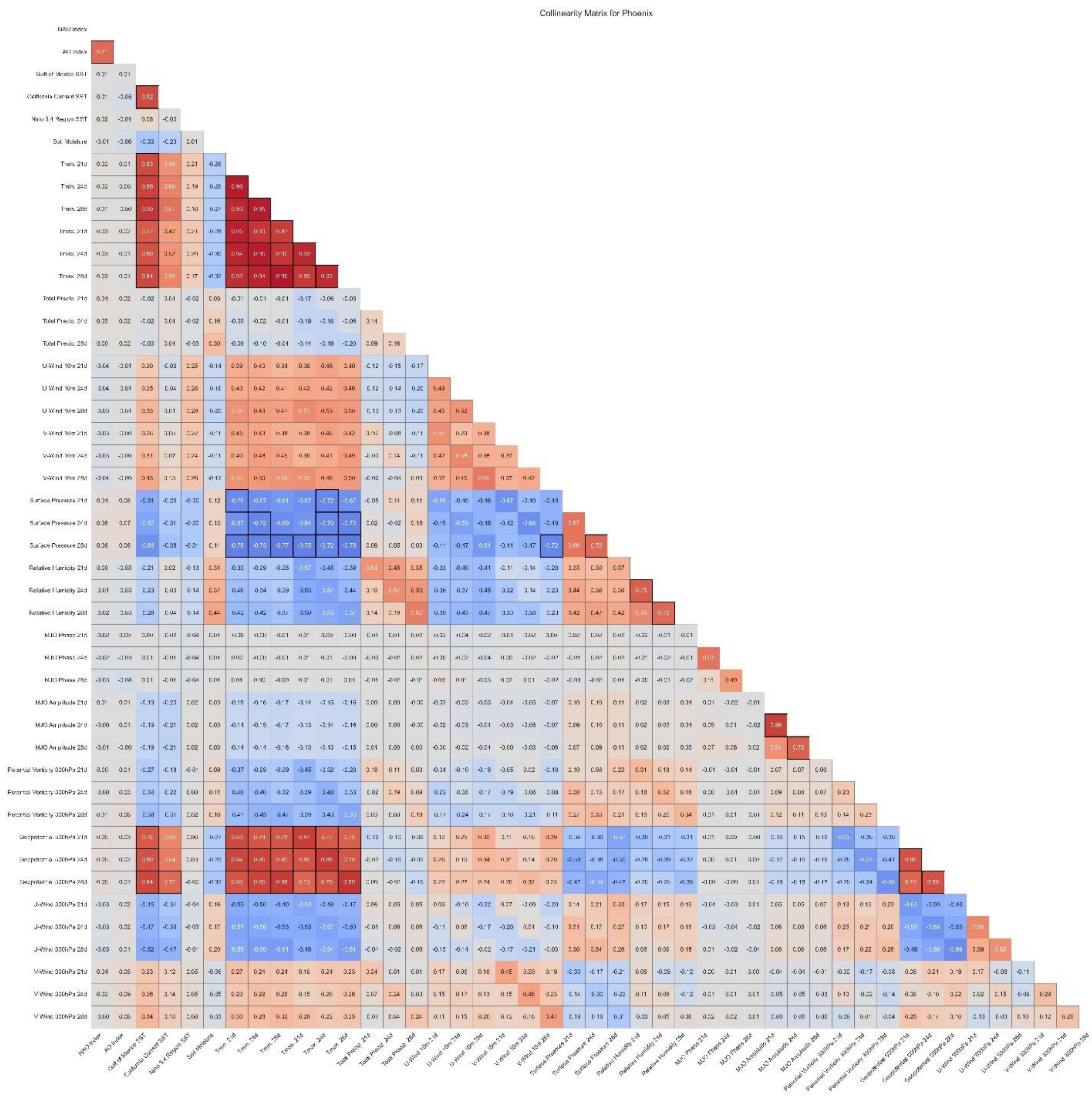
Collinearity Matrix for Phoenix

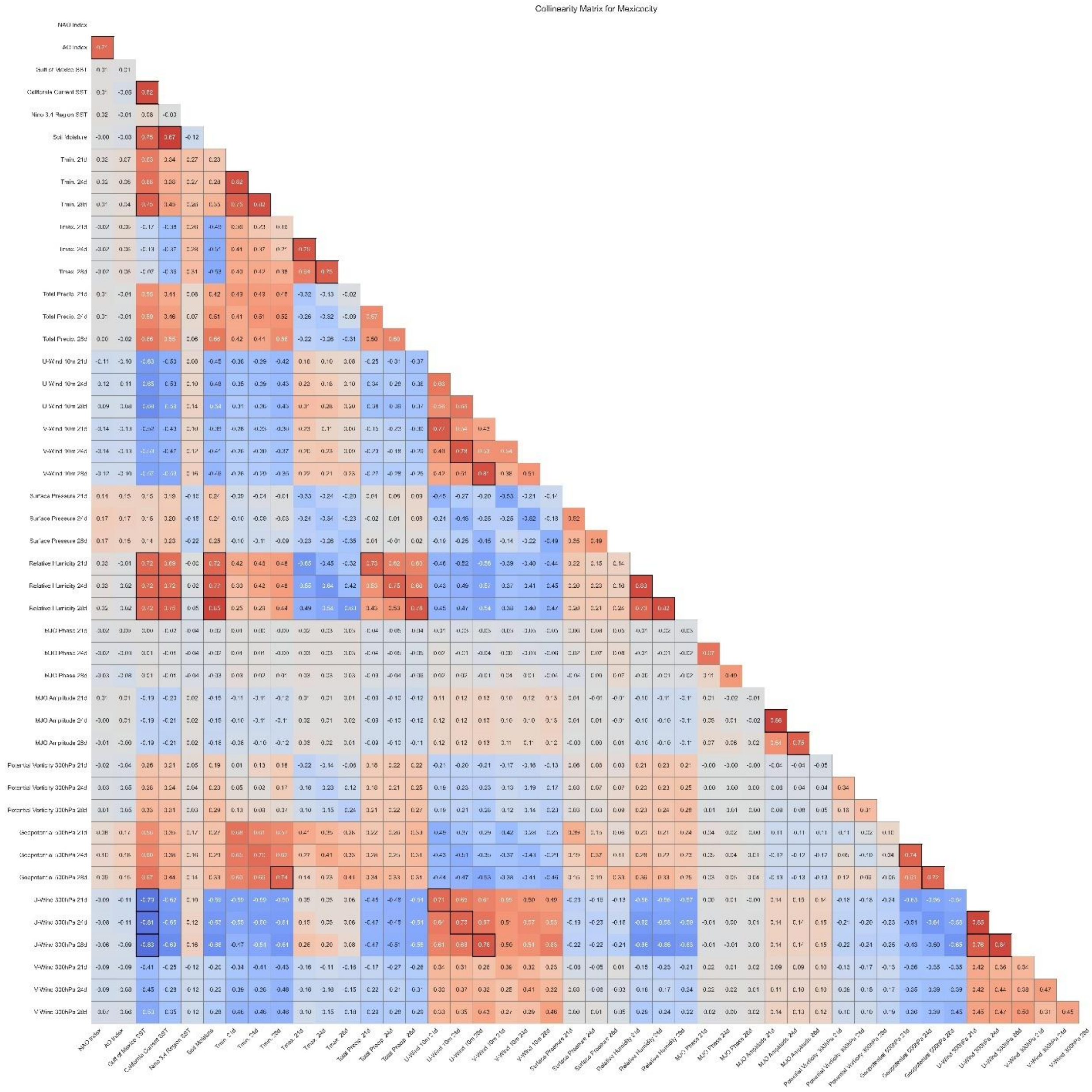

Collinearity Matrix for Mexicocity
NAO Index
AO Index
Gulf of Mexico SST
California Current SST
Nino 3.4 Region SST
Soil Moisture
Tmin 21d
Tmin 24d
Tmin 28d
Tmax 21d
Tmax 24d
Tmax 28d
Total Precip 21d
Total Precip 24d
Total Precip 28d
U-Wind 10m 21d
U-Wind 10m 24d
U-Wind 10m 28d
V-Wind 10m 21d
V-Wind 10m 24d
V-Wind 10m 28d
Surface Pressure 21d
Surface Pressure 24d
Surface Pressure 28d
Relative Humidity 21d
Relative Humidity 24d
Relative Humidity 28d
MJO Phase 21d
MJO Phase 24d
MJO Phase 28d
MJO Amplitude 21d
MJO Amplitude 24d
MJO Amplitude 28d
Potential Vorticity 300hPa 21d
Potential Vorticity 300hPa 24d
Potential Vorticity 300hPa 28d
Geopotential 500hPa 21d
Geopotential 500hPa 24d
Geopotential 500hPa 28d
U-Wind 300hPa 21d
U-Wind 300hPa 24d
U-Wind 300hPa 28d
V-Wind 300hPa 21d
V-Wind 300hPa 24d
V-Wind 300hPa 28d

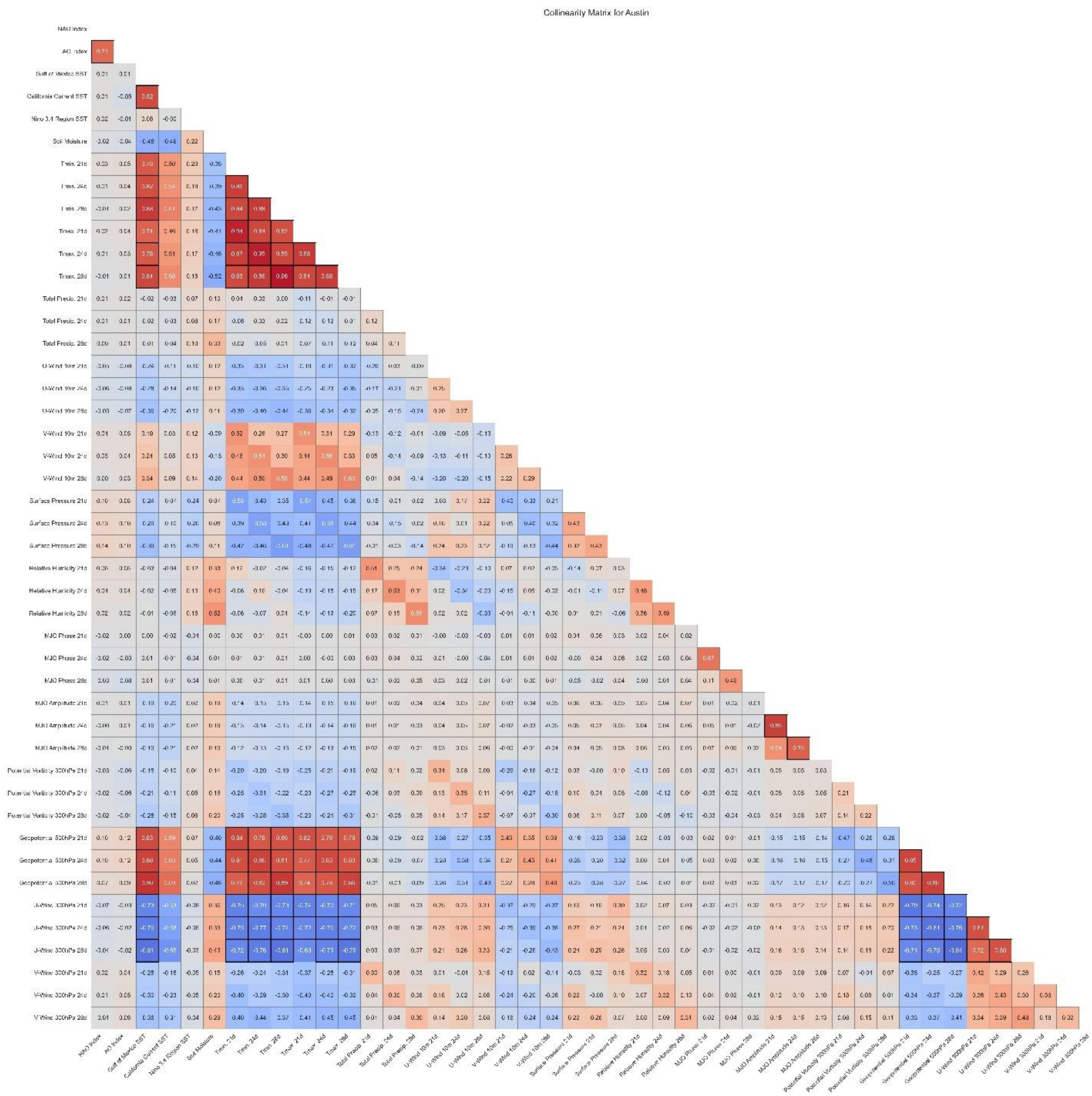
Collinearity Matrix for Austin
NAO Index
AO Index
Gulf of Mexico SST
California Current SST
Nino 3.4 Region SST
Soil Moisture
Tmin 21d
Tmin 24d
Tmin 28d
Tmax 21d
Tmax 24d
Tmax 28d
Total Precip 21d
Total Precip 24d
Total Precip 28d
U-Wind 10m 21d
U-Wind 10m 24d
U-Wind 10m 28d
V-Wind 10m 21d
V-Wind 10m 24d
V-Wind 10m 28d
Surface Pressure 21d
Surface Pressure 24d
Surface Pressure 28d
Relative Humidity 21d
Relative Humidity 24d
Relative Humidity 28d
MJO Phase 21d
MJO Phase 24d
MJO Phase 28d
MJO Amplitude 21d
MJO Amplitude 24d
MJO Amplitude 28d
Potential Vorticity 300hPa 21d
Potential Vorticity 300hPa 24d
Potential Vorticity 300hPa 28d
Geopotential 500hPa 21d
Geopotential 500hPa 24d
Geopotential 500hPa 28d
U-Wind 300hPa 21d
U-Wind 300hPa 24d
U-Wind 300hPa 28d
V-Wind 300hPa 21d
V-Wind 300hPa 24d
V-Wind 300hPa 28d